

Due to an error in the text on page S3, this ESI was updated on 13/12/2023

Supporting Information

Efficient Triplet Energy Transfer in 0D Metal Halide Hybrid with Long Persistence Room Temperature Phosphorescence for Time-Resolved Anti-Counterfeiting

Jie Li^{a, †}, Jingjie Wu^{b, †}, Yonghong Xiao^a, Longshi Rao^c, Ruosheng Zeng^{d, *}, Ke Xu^e,
Xiao-Chun Huang^a, Jin Z. Zhang^f and Binbin Luo^{a, *}

^a *Department of Chemistry and Chemical Engineering, Key Laboratory for Preparation and Application of Ordered Structural Materials of Guangdong Province, Shantou University, Shantou, 515063, P. R. China*

^b *Chaozhou Branch of Chemistry and Chemical Engineering Guangdong Laboratory, Chaozhou 521000, P. R. China*

^c *Department of Mechanical Engineering, College of Engineering, Shantou University, Shantou 515063, P. R. China*

^d *School of Physical Science and Technology, State Key Laboratory of Featured Metal Materials and Life-cycle Safety for Composite Structures, Guangxi University, Nanning 530004, P. R. China*

^e *Multiscale Crystal Materials Research Center, Shenzhen Institute of Advanced Technology, Chinese Academy of Sciences, Shenzhen 518055, P. R. China*

^f *Department of Chemistry and Biochemistry, University of California, Santa Cruz, California 95064, United States*

Corresponding Author: bbluo@stu.edu.cn

Table of Contents

Table of Contents.....	S2
Experimental section.....	S3
Table S1.....	S5
Figure S1.....	S6
Figure S2.....	S7
Figure S3.....	S8
Figure S4.....	S9
Table S2.....	S10
Figure S5.....	S11
Figure S6.....	S12
Figure S7.....	S13
Figure S8.....	S14
Table S3.....	S15
Figure S9.....	S16
Figure S10.....	S17
Table S4.....	S18
Table S5.....	S19
Figure S11.....	S20
Figure S12.....	S21
REFERENCE.....	S22

Experimental section

Materials

1H-Pyrazole-4-carbonitrile (98%, Adamas), hydrazine dihydrochloride (98%, Sigma-aldrich), indium acetate (99%, Aladdin), antimony(III) chloride (99%, Alfa Aesar), hydrazine hydrate (80%, Xilong Scientific), hydrochloric acid (37%, Guanghua Scientific), ethanol (AR, Guanghua Scientific), ethyl acetate (AR, Guanghua Scientific). All chemicals were used as supplied from commercial sources without further purification.

Synthesis of DPTA

First, 1H-Pyrazole-4-carbonitrile (1.00 g), hydrazine dihydrochloride (1.00 g), 1.00 mL hydrazine hydrate and 10.0 mL ethanol were mixed in a 48 mL glass vessel and heated at 130 °C for 12 h. After cooling to room temperature, the obtained yellow crystals were filtered and washed with water and ethanol. The obtained product was then dried at 50 °C for one day.

Synthesis of DIC Single Crystal and DIC:x%Sb Single Crystal

DIC was synthesized by loading 0.10 mmol DPTA, 0.10 mmol indium acetate into a 15.0 mL pressure bottle containing 3.00 mL HCl. After all reactants were dissolved at 120 °C in the sealed pressure bottle, the solution was cooled to room temperature without perturbation, and the DIC single crystal can be obtained after one day. For DIC:x%Sb samples, 0.10 mmol of DPTA, $x\% \times 0.1$ mmol of SbCl_3 and $(1-x\%) \times 0.1$ mmol of indium acetate were added into a 15.0 mL glass vessel containing 3 mL HCl. After all reactants were dissolved, the solution was cooled to room temperature without perturbation, and the DIC single crystal can be obtained after one day.

Characterization

Single crystal X-ray diffraction (SC-XRD)

SC-XRD tests were conducted on Rigaku XtaLab Pro MM007HF DWX diffractometer at 298 K and 100K using Cu $K\alpha$ radiation ($\lambda = 1.5418 \text{ \AA}$). The structures were solved by intrinsic phasing method using SHELXT¹ program implanted in Olex2². Refinement with full matrix least squares techniques on F2 was performed by using SHELXL³. Non-hydrogen atoms were anisotropic ally refined and all hydrogen atoms were generated based on riding mode.

Powder XRD

PXRD patterns were recorded on MiniFlex 600 (Rigaku) to examine the crystalline phase.

UV-vis absorption

UV-vis spectra were measured on Lambda 950 UV-vis Spectrometer (PerkinElmer).

Photoluminescence (PL) and excitation (PLE) spectra

Both of PL and PLE spectra were collected on PTI QM-TM (Photon Technology International).

Absolute PL quantum yield (QY)

Absolute PL QY was recorded on a HAMAMATSU C11347 spectrometer with integrating sphere with the excitation wavelength of 380 nm for all samples.

Inductively coupled plasma atomic emission spectrometry (ICP-AES)

ICP-AES was applied to detect the molar concentrations of Cd and Sb by using ICPE-9000, Shimadzu.

Scanning electron microscope (SEM) and Energy dispersive spectroscopy (EDS) mapping

SEM images and EDS mapping (JSM-7500F, JEOL) were carried out to obtain the morphology and elemental distribution.

Delayed PL and PL lifetime

Delayed PL and PL lifetime tests were collected on Edinburgh Instruments (FL 1000). The PL decay curves are fitted with exponential function as given in the following expression:

$$I(t) = \sum_n^{i=1} A_i e^{-\frac{t}{\tau_i}}$$

where $I(t)$ is the PL intensity at time t , A_i represents the relative weights of the decay components, τ_i denotes the decay time for the exponential components. The average lifetime is calculated based on the expression below:

$$\tau_{ave} = \frac{\sum_n^{i=1} A_i \tau_i^2}{\sum_n^{i=1} A_i \tau_i}$$

Computational methodology

To study band composition and band edge of the sample, first-principles calculations were carried out using density functional theory (DFT) as implemented in the VASP code.⁴⁻⁵ The projector augmented wave (PAW) method was used to describe the interaction between ions and electrons.⁶ The structural optimization were calculated using Perdew-Burke-Ernzerhof (PBE) exchange-correlation functional.⁷ The simulated model are modified by using primitive cell. The Brillouin zone integration was sampled with $4 \times 4 \times 4$ K-point meshes for static calculations. Following the space group of these structures, the K points of Brillouin region were referred to the symmetry of their space group to calculate band structure and density of states. The energy cutoff of plane-wave basis is 500 eV. The residual force of all atoms in the models was less than 0.02 eV/Å.

Table S1. Crystal data of DPTA.

Sample	DPTA
Empirical formula	C ₈ H ₈ N ₈
Formula weight	216.22
Temperature/K	297.99(10)
Radiation	Cu K α ($\lambda = 1.54178$)
Crystal system	Monoclinic
Space group	<i>Cc</i>
<i>a</i> /Å	4.79560(10)
<i>b</i> /Å	11.42880(10)
<i>c</i> /Å	16.8917(2)
α /°	90
β /°	96.7230(10)
γ /°	90
<i>V</i> /Å ³	919.43(2)
<i>Z</i>	4
ρ_{calc} (g/cm ³)	1.562
completeness to θ_{max}	100%
GOF	1.082
<i>R</i> _{int}	0.0231
final <i>R</i> indexes [<i>I</i> > 2 σ (<i>I</i>)] ^a	<i>R</i> ₁ = 0.0268, <i>wR</i> ₂ = 0.0694
<i>R</i> indexes (all data) ^a	<i>R</i> ₁ = 0.0270, <i>wR</i> ₂ = 0.0697
largest diff. peak and hole, e Å ⁻³	0.19/-0.15

^a $R_1 = \Sigma||F_o| - |F_c|| / \Sigma|F_o|$; $wR_2 = \{[\Sigma w(F_o^2 - F_c^2)^2] / \Sigma[w(F_o^2)^2]\}^{1/2}$; $w = 1/[\sigma^2(F_o^2) + (aP)^2 + bP]$, where $P = [\max(F_o^2, 0) + 2F_c^2] / 3$ for all data.

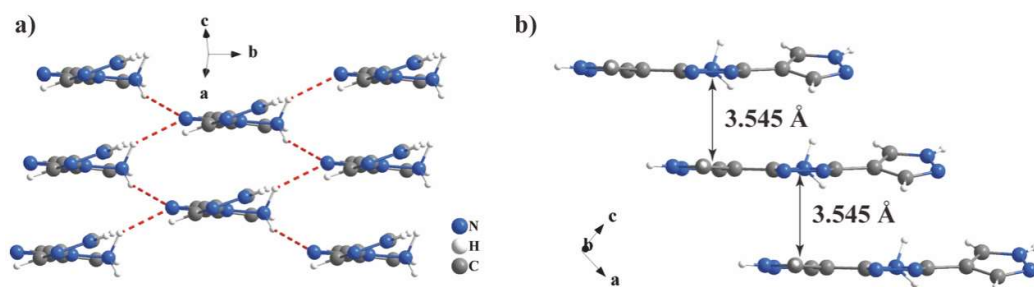


Figure S1. (a) Intermolecular hydrogen-bonding interaction and perpendicular distance for DPTA single crystals.

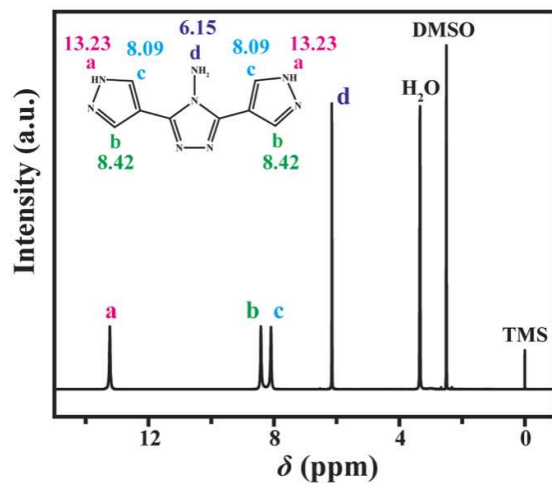


Figure S2. ¹H NMR spectrum of DPTA dissolved in *d*₆-DMSO, DMSO and TMS are denoted to dimethyl sulphoxide and tetramethylsilane, respectively.

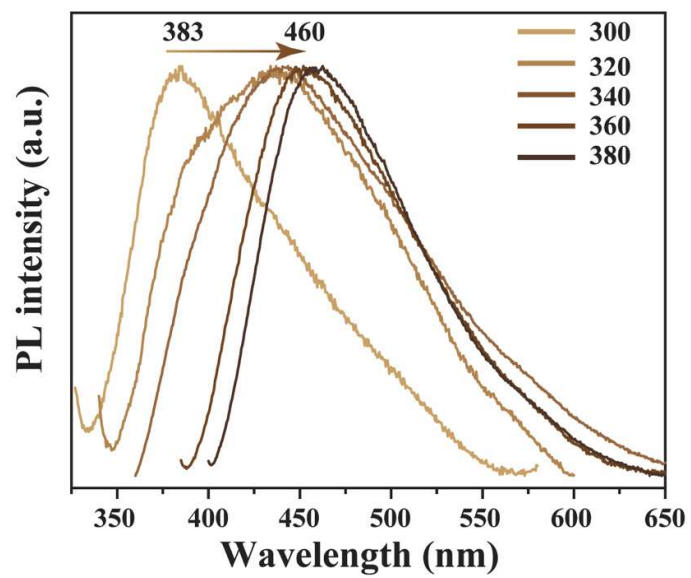


Figure S3. Excitation-dependent PL of DPTA powders.

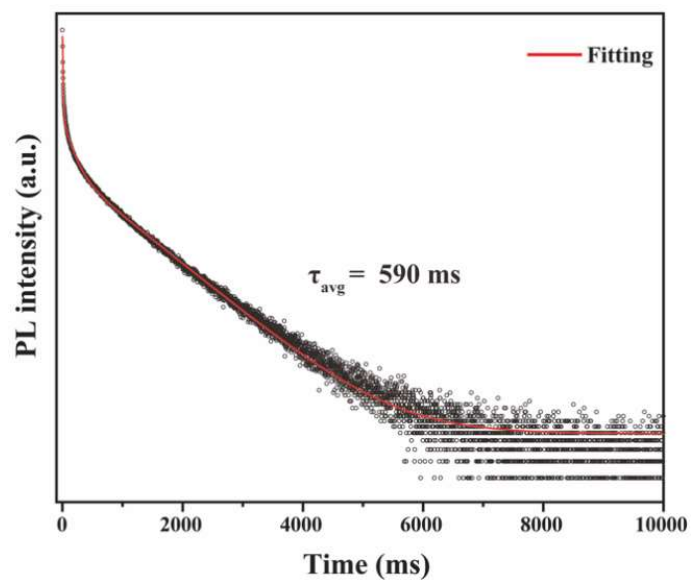


Figure S4. PL decay curves of DPTA monitoring at 518 nm with excitation at 365 nm.

Table S2. Crystal data of DIC.

Sample	DIC
Empirical formula	C ₈ H ₁₆ Cl ₆ InN ₈ O _{2.5}
Formula weight	591.81
Temperature/K	297.99(10)
Radiation	Cu K α ($\lambda = 1.54178$)
Crystal system	Triclinic
Space group	$P\bar{1}$
$a/\text{\AA}$	7.9545(3)
$b/\text{\AA}$	8.1351(3)
$c/\text{\AA}$	8.1882(3)
$\alpha/^\circ$	106.557(3)
$\beta/^\circ$	105.950(3)
$\gamma/^\circ$	92.161(3)
$V/\text{\AA}^3$	484.46(3)
Z	1
ρ_{calc} (g/cm ³)	2.029
completeness to θ_{max}	99.3%
GOF	1.142
R_{int}	0.0168
final R indexes [$I > 2\sigma(I)$] ^a	$R_I = 0.0205$, $wR_2 = 0.0553$
R indexes (all data) ^a	$R_I = 0.0206$, $wR_2 = 0.0553$
largest diff. peak and hole, e \AA^{-3}	0.59/-0.58

^a $R_I = \Sigma||F_o| - |F_c||/\Sigma|F_o|$; $wR_2 = \{[\Sigma w(F_o^2 - F_c^2)^2]/\Sigma[w(F_o^2)^2]\}^{1/2}$; $w = 1/[\sigma^2(F_o^2) + (aP)^2 + bP]$, where $P = [\max(F_o^2, 0) + 2F_c^2]/3$ for all data.

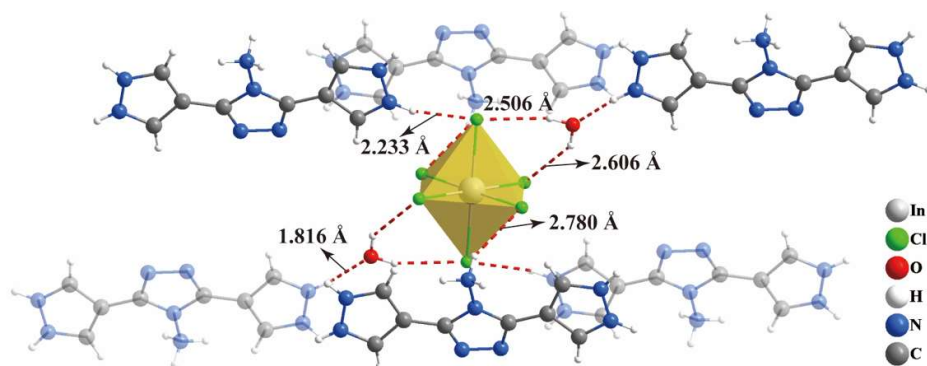


Figure S5. Water-mediated hydrogen-bonding network in DIC.

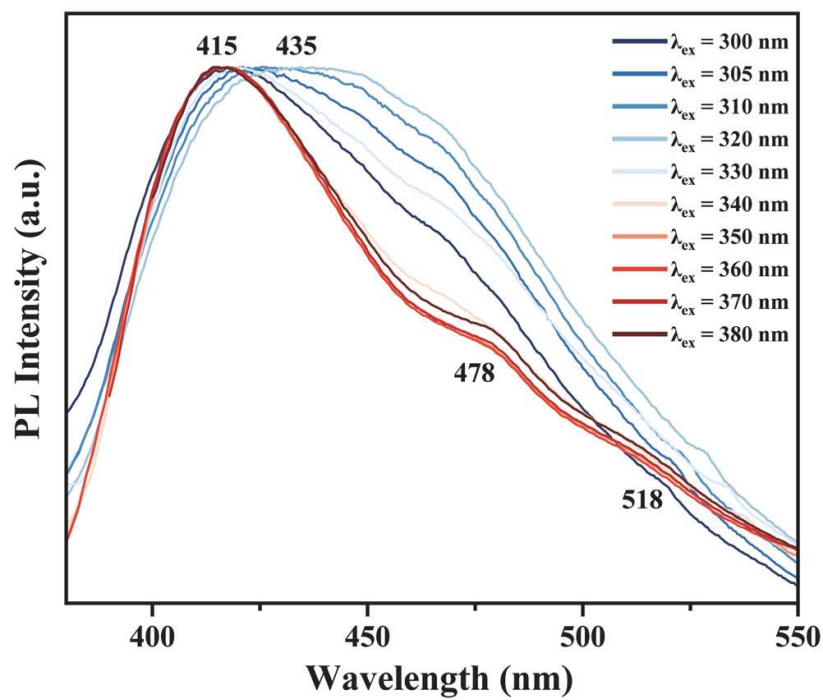


Figure S6. Excitation-dependent PL of DIC powders.

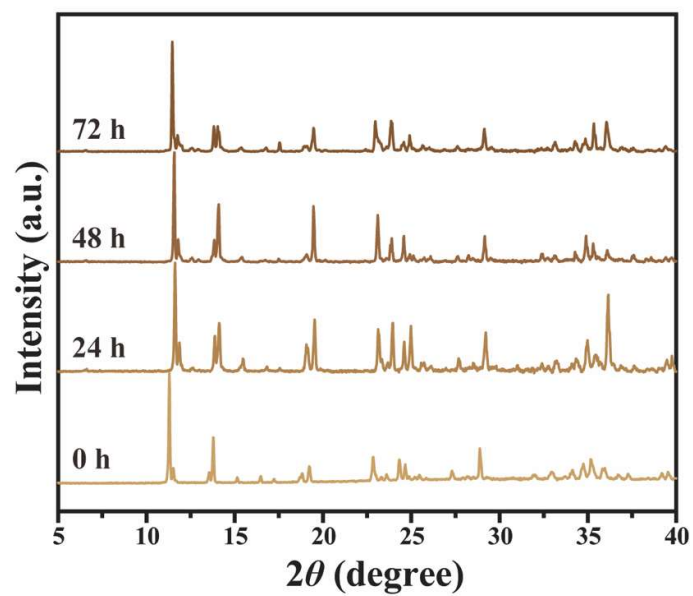


Figure S7. XRD patterns of DIC under open air for different hours.

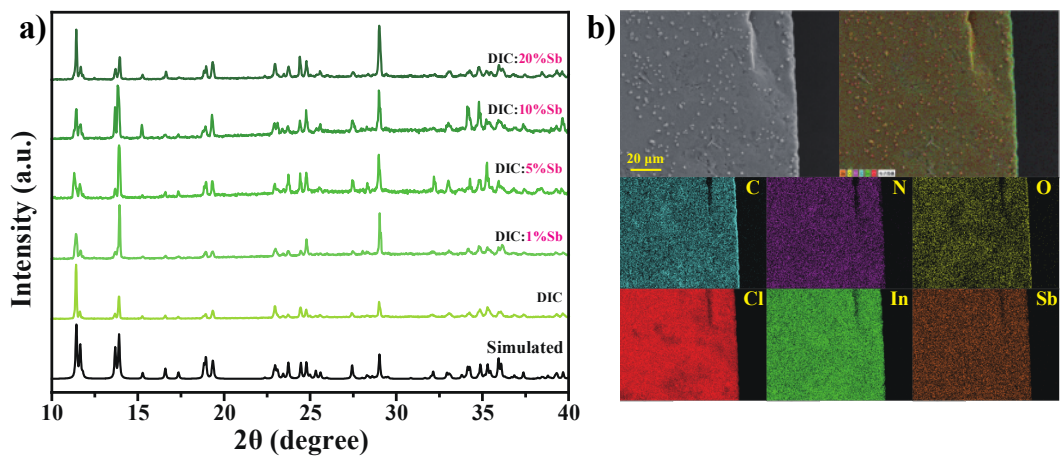


Figure S8. (a) XRD of DIC:x%Sb with different Sb doping levels and (b) EDS mapping of DIC:10%Sb.

Table S3. Sb³⁺ contents of DIC:x%Sb detected through ICP-AES.

Samples	Sb atomic ratio
DIC:1%Sb	0.38%
DIC:5%Sb	1.34%
DIC:10%Sb	2.48%
DIC:20%Sb	4.77%

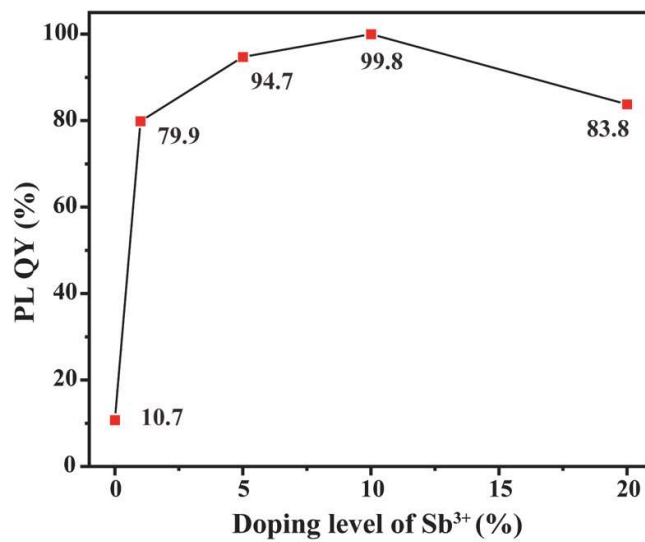


Figure S9. PLQY of DIC:x%Sb with different doping levels.

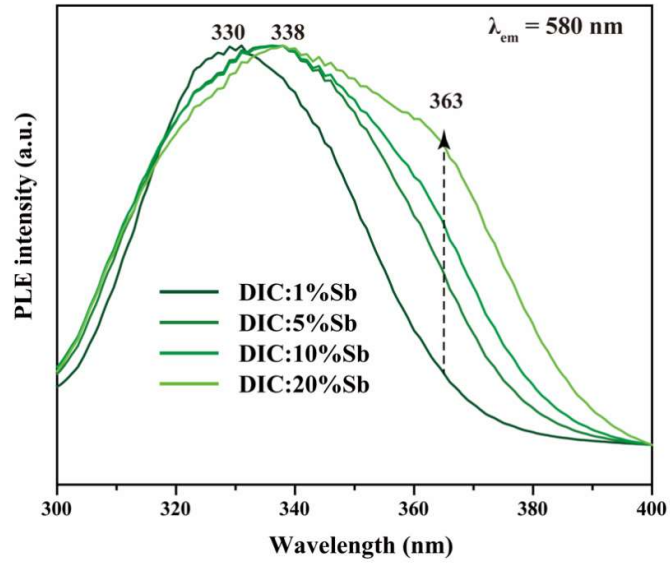


Figure S10. PLE spectrum of DIC:x%Sb monitoring at 580 nm.

Table S4. Fitting parameters of time-resolved PL for DPTA and DIC:x%Sb at 518 nm.

Sample	A ₁	τ_1 (ms)	A ₂	τ_2 (ms)	A ₃	τ_3 (ms)	τ_{avg} (ms)	Φ_{TET}
DPTA	0.86	9.8	0.09	147	0.05	845	590	-
DIC	0.74	11.9	0.25	65	0.01	650	170	-
DIC:1%Sb	0.61	10.5	0.38	55	0.01	500	115	32.4%
DIC:5%Sb	0.57	9.0	0.42	58	0.01	330	77	54.7%
DIC:10%Sb	0.45	4.8	0.54	55	0.01	300	73	57.1%
DIC:20%Sb	0.39	3.3	0.6	48	0.01	230	59	65.3%

Table S5. Fitting parameters of time-resolved PL for DIC:x%Sb at 580 nm.

Sample	A_1	τ_1 (μs)	A_2	τ_2 (μs)	A_3	τ_3 (μs)	τ_{avg} (μs)
DIC:1%Sb	0.778	2.8	0.221	9.9	0.001	119	7.7
DIC:5%Sb	0.513	3.4	0.486	8.4	0.001	154	10.3
DIC:10%Sb	0.572	3.2	0.427	8.3	0.001	229	10.8
DIC:20%Sb	0.662	3.1	0.337	8.7	0.001	302	13.3

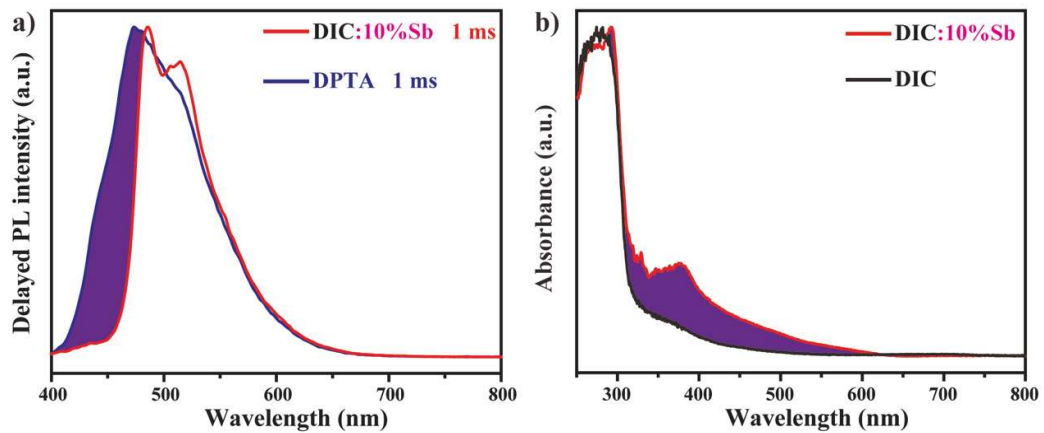


Figure S11. The difference (marked with purple) of (a) delayed PL and (b) absorption spectrum among DPTA, DIC and DIC:10%Sb.

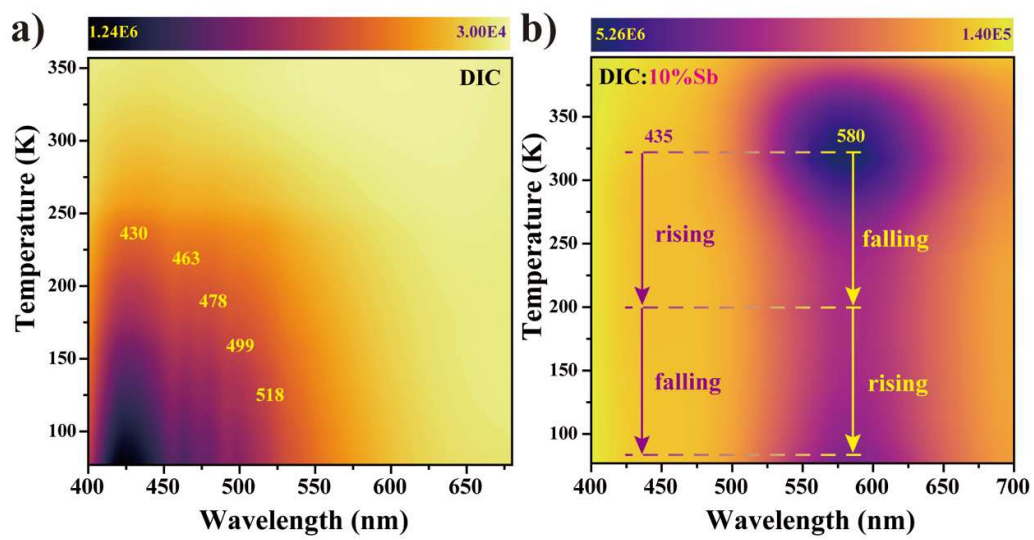


Figure S12. Temperature-dependent PL of (a) pristine DIC and (b) DIC:10%Sb.

REFERENCES

1. Sheldrick, G. M., Shelxt - Integrated Space-Group and Crystal-Structure Determination. *Acta Cryst. A* **2015**, *71*, 3-8.
2. Dolomanov, O. V. B., L. J.; Gildea, R. J.; Howard, J. A. K.; Puschmann, H., Olex2: A Complete Structure Solution, Refinement and Analysis Program. *J. Appl. Crystallogr.* **2009**, *42*, 339-341.
3. Sheldrick, G. M., A Short History of Shelx. *Acta Cryst. A* **2008**, *64*, 112-122.
4. Furthmüller, G. K. a. J., Efficient Iterative Schemes for Ab Initio Total-Energy Calculations Using a Plane-Wave Basis Set. *Phys. Rev. B* **1996**, *54*, 11169-11186.
5. Joubert, G. K. a. D., From Ultrasoft Pseudopotentials to the Projector Augmented-Wave Method. *Phys. Rev. B* **1999**, *59*, 1758-1775.
6. Blöchl, P. E., Projector Augmented-Wave Method. *Phys. Rev. B* **1994**, *50*, 17953-17979.
7. John P. Perdew, K. B., and Matthias Ernzerhof, Generalized Gradient Approximation Made Simple. *Phys. Rev. Lett.* **1996**, *77*, 3865-3868.